УДК 96.40.DE

Plyasheshnikov A. V., Aharonian F. A., Hemberger M., Hofmann W., Konopelko A. K., Völk H. J.

Imaging Air Cherenkov Technique and Mass Composition of Primary Cosmic Rays

Imaging atmospheric Cherenkov telescopes (IACT) have proven to be up to now the most effective instruments for the observation of primary TeV γ-radiation from astrophysical objects. The high detection rate as well as the capability of accurate reconstruction of air shower parameters by the IACT technique also allow the use of the imaging technique for the study of the energy spectrum and mass composition of cosmic rays. In this paper we discuss the potential of this technique for the separation of different components of cosmic rays in the energy region from 1 to 100 TeV/amu. We show that the imaging technique allows adequate separation of showers produced by protons from the contributions of all other nuclei, including α-particles, and thus allows a measurement of the energy spectrum of the proton component at TeV energies. Such measurements can be performed by currently operating single IACTs designed originally for γ-ray astronomical purposes. The effective separation of different nucleus groups of the cosmic radiation is a more difficult problem. It benefits from the stereoscopic reconstruction of the shower development in the Earth's atmosphere. Our calculations show that simultaneous detection of air showers by 2 IACTs located at a distance of about 100 m from each other allows an effective separation of the proton, α-particle, M (O), H (Si), and VH (Fe) groups of cosmic ray nuclei.

Introduction

The recent observations of TeV γ-radiation from several astrophysical sources convincingly demonstrate the high performance of imaging atmospheric Cherenkov telescopes (IACTs), and set a solid basis for ground-based gamma ray astronomy (see e.g. [1]). Remarkable features of the IACT technique are the high detection rate, and the ability of accurate reconstruction of air shower parameters. The differences in the development of electromagnetic and hadron showers are transfered to their Cherenkov images, which ultimately results in an effective separation of γ-ray and cosmic ray (CR) induced showers (see e.g. [2]). The images of γ-ray showers are compact and regular compared with images of hadron showers. It is remarkable that there is also a difference between images of hadron showers produced by different groups of CRs. Due to larger cross-sections of interaction ($\sigma \propto A^{\alpha}$; $\alpha \simeq 2/3$) and faster degradation of the energy the altitude of the shower maximum position increases rapidly with A. Thus the determination of the shower maximum using the angular distribution [3] or the time structure [4] of the Cherenkov radiation of showers yield methods for the measurement of the chemical composition of CRs at energies above 100 TeV/amu.

In addition, due to the very rapid (exponential) decrease of the air density with the altitude, the showers initiated by nuclei have a significantly broader radial distribution than the proton – induced showers. Therefore in the focal plane of a Cherenkov telescope the size of the image increases with the atomic number A of the primary particle and one may conclude that the currently operating telescopes should be able to make an important contribution to the measurement of the mass composition of CRs of energies from 1 to 100 TeV/amu. Such a study could be considered as a complementary approach to the satellite- and balloon-borne experiments in that energy region.

In this paper we present Monte Carlo calculations of the Cherenkov radiation from air showers produced by different groups of CR nuclei, and determine the image parameters that are most sensitive to the atomic number of the primary nuclei. The method of separation of showers produced by different nuclei is based on the second-moment parameterization of the Cherenkov images currently used in the observation of TeV γ-ray sources (see e.g. [5]). Due to the isotropic distribution of CR images in the focal plane of the telescope, only the shape parameters of the image can be invoked for such analysis. We show that in the case of a single IACT the so called *Width* parameter, characterizing the lateral development of the shower, allows to distinguish the proton component from heavier nuclei (including α-particles) and thus to measure the spectrum of CR protons with high accuracy. The combination of *Width* with other parameters (the intrinsic fluctuations of the image intensity, *Length*, *Size*, *Density*, etc.) makes it possible to separate nuclei with significantly different atomic numbers A, for example, protons and α-particle from the

Table 1

Data on the mass composition used in our analysis

Group of nuclei	p	α	**M**	**H**	**VH**
Mean atomic number, A	1	4	16	28	56
Chemical symbol	H	He	O	Si	Fe
Percentage of nuclei	38	18	15	20	9

nuclei of the (CNO) group and heavier ones.

Simultaneous detection of showers by several IACTs, sufficiently separated from each other, gives information about the shower development in different projections, and allows the determination of the distance to the core of each individual shower. This improves significantly the efficiency of nuclei identification, and allows the flux evaluation for 5 different groups of CR nuclei: p, α, (CNO), Si, Fe.

1. Simulations

We used two different computational codes to obtain the simulation results analyzed in this paper. The first one is a modified version of the code described in [6,7], which includes simulations of both the electromagnetic and hadron cascades. In addition, for a study of the sensitivity of the results to the basic features of the nuclear interaction models, in the stage of simulations of hadron cascades, we have used the version 4.50 of the CORSIKA code [8] in which the cross-sections of hadron interactions based on recent accelerator data and theoretical models are implemented in great detail.

In total, 10^5 showers, produced by protons, α-particles, oxygen, silicon and iron nuclei, have been simulated in the energy range of primary particles from 0.5 to 100 TeV/amu. The simulations were carried out for telescopes similar to the HEGRA IACTs with 8.5 m^2 optical mirror, and equipped with 271-pixel cameras with a pixel size 0.24° and a field of view $\simeq 4.6°$. The pixel size of the camera is sufficiently small [9] to avoid distortion of the image shape parameters caused by the finite granularity of the camera. To diminish a distortion of images due to the limited field of view of the camera [9] we take in the analysis only images having the center of gravity within the central ($\simeq 3°$) part of the camera. The calculations have been done for a single telescope, and for 2 telescopes separated by 85 m and operating in coincidence.

For the detection of showers we apply the trigger condition $2/91 > q_0$: at least two pixels from the central ($\simeq 3°$) part of the camera should exceed a threshold q_0. The minimum acceptable value of q_0 is determined by the demand for a reliable suppression of the night sky background (*N.S.B.*). For a single telescope we use $q_0 \simeq 15$ ph. e. For 2 telescopes in coincidence the threshold can be reduced to $q_0 \leq 10$ ph. e. However, below (except for Table 11 and Figure 7) we apply a higher *software trigger*, $q_0 = 30$ ph. e., i.e. we analyze only events containing large number of photoelectrons, which allows the reduction of fluctuations of the image parameters.

For the evaluation of the basic image parameters we use the standard second-moment approach [10]. To reduce the influence of the *N.S.B.* on the image parameters, only the pixels containing more than $m_0 = 4$ ph. e. are included in the image parametrization.

Although the energy spectra of different groups of CRs are slightly different [11], we use here for simplicity an all-particle flux of CRs in the form

$$dF_{CR}/dE = 0.25 \cdot E^{-2.7} (s \cdot sr \cdot m^2 \cdot TeV)^{-1}, \quad (1)$$

assuming an energy–independent contribution of different groups of nuclei to the total CR flux (see Table 1).

We simulate showers produced by 5 species of primary nuclei (p, α, O, Si and Fe), and assume that all showers of the **M**edium, **H**eavy, and **V**ery **H**eavy groups are induced by nuclei with the same value of the atomic number, corresponding to O, Si, and Fe, respectively.

2. Collection area and detection rates

In Figure 1a we show the collection areas of a single IACT for different groups of CR nuclei calculated in accordance with [12]. For all primary nuclei the collection area increases with the energy of particle. While in the low energy regime the light nuclei are detected more effectively than the heavy ones, at high energies the values of the collection area become comparable for all nuclei. In Figure 1b we show the differential detection rates of CRs, i.e. the product of the collection area and the differential energy spectrum. The *effective energy threshold* of shower detection E_{th}, defined as the energy at which the differential detection rate reaches its maximum, increases strongly with the atomic number of the primary particles (approximately as $\propto A^{0.5}$). The values of E_{th} for different nuclei are presented in Table 2.

The integral detection rate of cosmic rays, $R_{\rm tot}$, can be presented as the sum of the partial integral detection rates, $R_{\rm j}$, corresponding to individual group of CR nuclei:

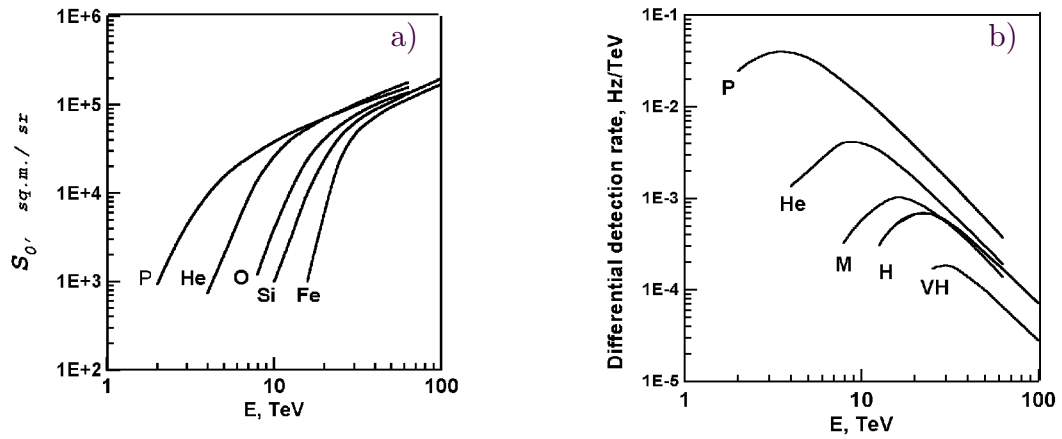

Figure 1. The energy dependence of the collection area S (a) and differential detection rate (b). $S_o = S/\Omega$, Ω is the solid angle corresponding to the central ($\simeq 3^o$) part of the camera

$$R_{tot} = \sum_{j=1}^{J} R_j \qquad (2)$$

where $J = 5$ is the total number of groups.

In Table 3 we present the contributions of air showers from different groups of nuclei to the integral detection rate of CRs. One can see that the increase of $E_{\rm th}$ with the atomic number reduces the portion of heavy nuclei in the detection rate compared to their portion in the primary cosmic radiation. In particular, while the proportion of the Fe group nuclei is about 9% in the total CRs (see Table 1), their contribution to the detection rate is less than 3%. Nevertheless, even for the VH group the IACT technique gives a good statistics for reasonable observation times. For example, for several hundred hours of the observation, during approximately one year telescope operation, we expect approximately 3×10^5 detected showers produced by VH nuclei. In Table 3 we also show the relative detection rates for air showers detected simultaneously by two identical IACTs separated from each other by 85 m. In comparison with a single telescope a slight increase of the detection rates of heavy nuclei is observed, which can be explained by a flatter lateral distribution of the Cherenkov radiation from the showers produced by the heavy nuclei compared with that from proton-induced showers.

3. Dependence of image parameters on atomic number

A successful application of the IACT technique to the analysis of the CR mass composition is possible only if the Cherenkov light image parameters

Table 2

The effective energy threshold of detection of CR nuclei by a single IACT.

Primary nucleus	P	α	O	Si	Fe
E_{th} [TeV]	3.2	8.5	15.4	20.4	25.1

Table 3

The contribution of different groups of CR nuclei to the total detection rate

Group of nuclei	P	α	M	H	VH	α – VH
Single IACT	72.7	15.3	5.4	5.0	1.6	27.3
2 IACT system	67.1	16.8	7.2	6.7	2.4	32.9

are sensitive to the atomic number A of the primary nucleus.

In Figures 2 we show the probability distributions for the second-moment parameters *Length* and *Width*, which characterize the longitudinal and lateral development of the showers in the atmosphere, respectively. One can see from Figure 2a that the probability distribution of the *Width* parameter exhibits a quite strong dependence on A. In particular, the most probable value of *Width* increases from 0.20° for protons to 0.35° for iron nuclei. Similarly, the average value of the *Length* parameter increase from 0.44° for proton-induced showers to 0.55° for iron-induced showers (as a consequence of this behaviour, the characteristic angular size of the image, $(Length \cdot Width)^{1/2}$, also increases with A). These two parameters provide different efficiences for the separation of the show-

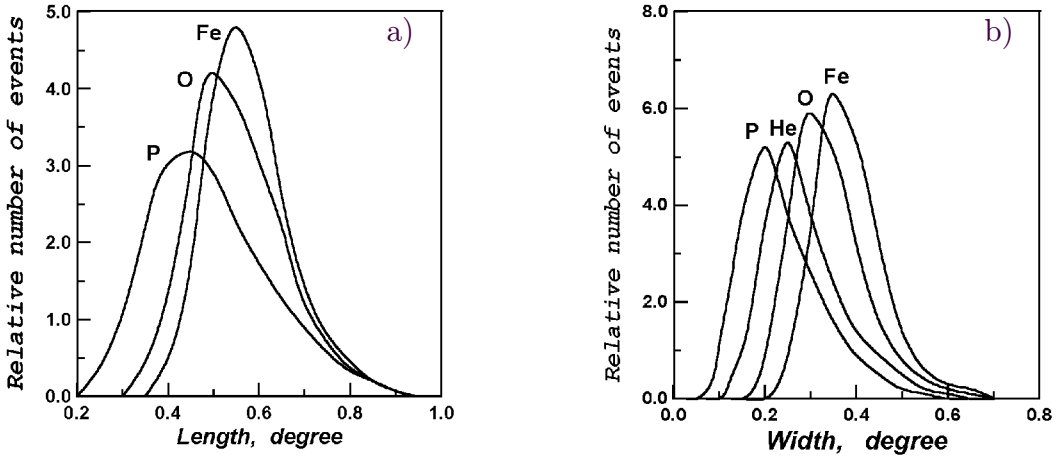

Figure 2. Probability distributions of *Length* (a) and *Width* (b) parameters for air showers created by different nuclei

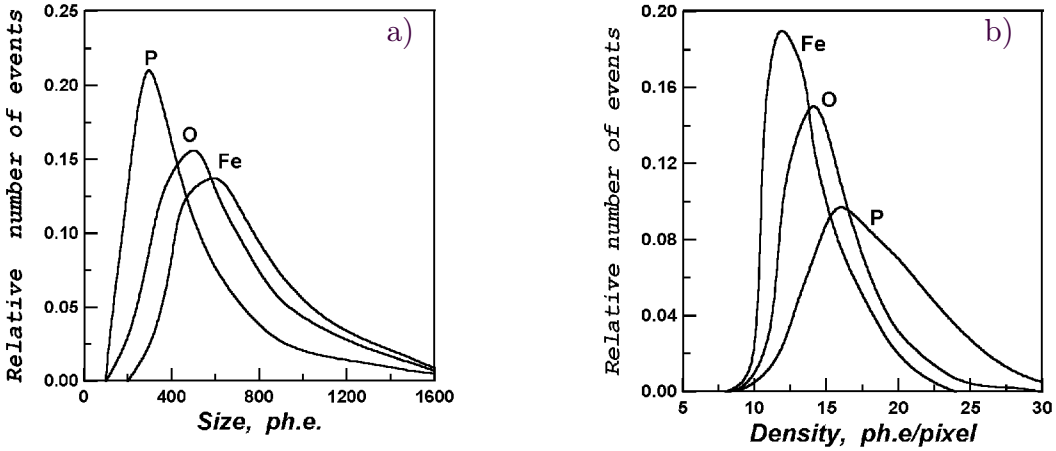

Figure 3. Probability distributions of *Size* (a) and *Density* (b) parameters for air showers created by different nuclei

ers of different origin. Due to the narrower distributions of the *Width* parameter, the overlap of the curves representing different groups of nuclei is less than for distributions on the *Length* parameter (compare Figures 2a and 2b). Moreover, these two parameters strongly correlate with each other. Thus after use of the *Width* parameter, the application of the *Length* parameter does not significantly improve the separation efficiency.

In Figures 3 we present the probability distributions for two other parameters, relatively sensitive to variations in A: (1) the *Size* parameter, determined as the total number of photoelectrons in the image; (2) the *Density* of the image, $Density = Size/N$, where N is the number of pixels used for the image parametrization. One can see that the light nuclei are characterized by smaller values of the *Size* parameter and larger values of the *Density* parameter.

The fluctuations in the development of air showers decrease noticeably with the growth of the atomic number of the primary nucleus (see e.g., [13]). Therefore, one should expect a noticeable anticorrelation between the atomic number and the intrinsic fluctuations of the light intensity of the image. If so, then the analysis of the parameters characterizing the fluctuations of the image shape should increase the efficiency of separation of different groups of primary nuclei. In this paper we use the χ^2 parameter of the two-dimensional angular distribution of images which is described in the Appendix. The χ^2 distributions of for proton– and Fe–induced showers detected by a single telescope are shown in Figure 4. Iron nuclei are assigned for selection in this figure.

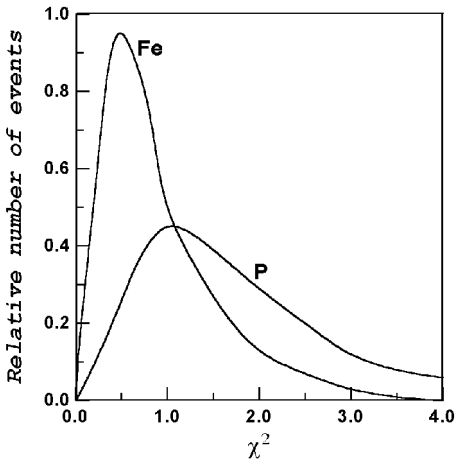

Figure 4. The probability distributions for the χ^2_w-parameter

4. Measurement of elemental composition

Suppose that we want to select from the data set those events corresponding to a definite group of nuclei (for example, the i-th nucleus group). For this purpose we apply to every event the set of selection criteria based on the image parameters discussed above. As an output of this procedure we get a reduced data set enriched by events of the i-th nucleus group. Consequently, we have instead of (2) the following equation:

$$\tilde{R}^{(i)}_{tot} = \sum_{j=1}^{J} \tilde{R}^{(i)}_{j} = \sum_{j=1}^{J} \kappa^{(i)}_{j} \cdot R_j \qquad (3)$$

where $\tilde{R}^{(i)}_{tot}$, $\tilde{R}^{(i)}_{j}$ are the total and partial detection rates of the IACT after the selection procedure (hereafter the *residual detection rates*), $\kappa^{(i)}_{j}$ is the probability for nuclei of the j-th group to satisfy selection conditions tailored to the i-th group (hereafter the *acceptance probability*).

Application of the procedure described above to all basic groups of nuclei leads to a system of equations:

$$\sum_{j=1}^{J} \kappa^{(i)}_{j} \cdot R_j = \tilde{R}^{(i)}_{tot}, \qquad i = 1, 2, \ldots, J \qquad (4)$$

which can provide the basis for the analysis of mass composition. To carry out this analysis one should establish for each basic group of nuclei a selection criterion and obtain from the simulation data a two-dimensional array of acceptance probabilities – $\kappa^{(i)}_{j}$. After that, the identical criteria are applied to the observational data to yield the quantities $\tilde{R}^{(i)}_{tot}$, $i = 1, 2, \cdots, J$. Substituting $\tilde{R}^{(i)}_{tot}$ in (4) and solving these equations one can get the initial detection rates R_j, $j = 1, 2, \cdots, J$. Finally, comparing R_j with theoretical predictions (for example, with data of Table 3) the mass composition can be determined.

A crucial issue is the choice of optimum selection criteria. A selection criterion is effective only if its application enhances the percentage of the group assigned for separation. In this regard, let us use the relations

$$P_j = 100 \cdot R_j / R_{tot}, \quad \tilde{P}^{(i)}_{j} = 100 \cdot \tilde{R}^{(i)}_{j} / \tilde{R}^{(i)}_{tot}, \quad j = 1, 2, \cdots, J \qquad (5)$$

where P_j and$\tilde{P^{(i)}_{j}}$ denote the percentage of events of different groups of nuclei in the total detection rate before and after selection of the i-th group, respectively, and use as a total measure of the sep-

Table 4

Selection of CR protons on the basis of criterion $w < w_o$ for a single IACT

w_o	0.14^o	0.16^o	0.20^o	0.24^o	0.28^o	∞
κ_P	0.106	0.187	0.392	0.580	0.725	1.000
κ_α	0.008	0.034	0.138	0.345	0.552	1.000
κ_O	0.000	0.000	0.016	0.082	0.253	1.000
κ_{Si}	0.000	0.000	0.001	0.030	0.150	1.000
κ_{Fe}	0.000	0.000	0.000	0.005	0.045	1.000
$\tilde{P}_P$	98.5	96.3	92.8	87.8	83.3	72.7

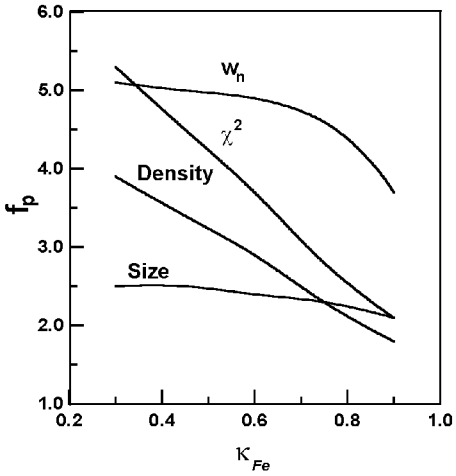

Figure 5. Results on an independent application of selection criteria for a single telescope

aration efficiency the enrichment factor

$$\eta = \tilde{P}_i^{(i)}/P_i. \quad (6)$$

Imagine that we deal with equal numbers of events, N_o, corresponding to the i-th and j-th groups of nuclei. Let us denote as $N^{(i)}, N^{(j)}$ the mean numbers of accepted events after selection of the i-th group and then use the suppression factor

$$f_j^{(i)} = N^{(i)}/N^{(j)} = \\ = (N^{(i)}/N_o)/(N^{(j)}/N_o) = \kappa_i^{(i)}/\kappa_j^{(i)}. \quad (7)$$

as a measure of rejection of events of the group j.

5. Selection criteria and separation efficiency

In this section we discuss the selection efficiency of different groups of nuclei for a single IACT with parameters described above and for a stereoscopic system consisting of two identical telescopes separated by a distance of 85 m.

Single IACT

In Figure 5 we show the results of an independent application of different selection criteria to two populations of cosmic rays – protons and iron nuclei. Iron nuclei are assigned here for selection (signal), and proton–induced showers are considered as a background (noise). It is seen that the *Width* and χ^2 parameters provide most effective criteria for the suppression of the proton–induced showers. Independent application of the *Size* and *Density* cuts shows less efficiency. Furthermore, these parameters strongly correlate with the *Width* parameter, and their application do not improve significantly the nuclei separation efficiency after the application of the *Width* cuts.

In Table 4 we show the acceptance probabilities corresponding to the criterion based only on the *Width (w)* parameter. It is seen that even for a single IACT this parameter provides an extraction of the proton component. The percentage of protons ($\tilde{P}_p$) in the residual detection rate grows rapidly with reduction of w_o. For example, for $w_0 = 0.14^\circ$, 98.5% accepted events are air showers generated by protons, 1.5% – by α-particles; all other groups of nuclei are practically completely excluded. Consequently, the IACT technique can be successfully applied to study the spectrum of CR protons. This would allow an independent test of possible spectral changes of the proton component of CRs in the energy region 1-10 TeV recently reported by two different groups based on the data obtained by satellite- and balloon-borne experiments [14,15].

The results concerning contribution of heavier nuclei to the CR flux based on the single IACT data are summarized in Tables 5 (for the Fe group) and 6 (for the (CNO) group). We conclude that a simultaneous application of several parameters cuts essentially improves the separation efficiency compared with independent application of any of these parameters. In particular, suppression factors for protons $f_p \simeq 38.3$ and $\simeq 9.2$ can be achieved with acceptance probabilities for the Fe nuclei and the (CNO) group of $\kappa_{Fe} = 0.115$ and $\kappa_O = 0.055$, respectively.

Stereoscopic IACT system

The distributions of air shower parameters are determined by the intrinsic fluctuations of the shower development due to the stochastic nature of interactions of the high energy particles in the Earth's atmosphere. This results in a significant overlap of the distributions of the image parameters characterizing showers produced by different nuclei. Ultimately this is the limit for the sepa-

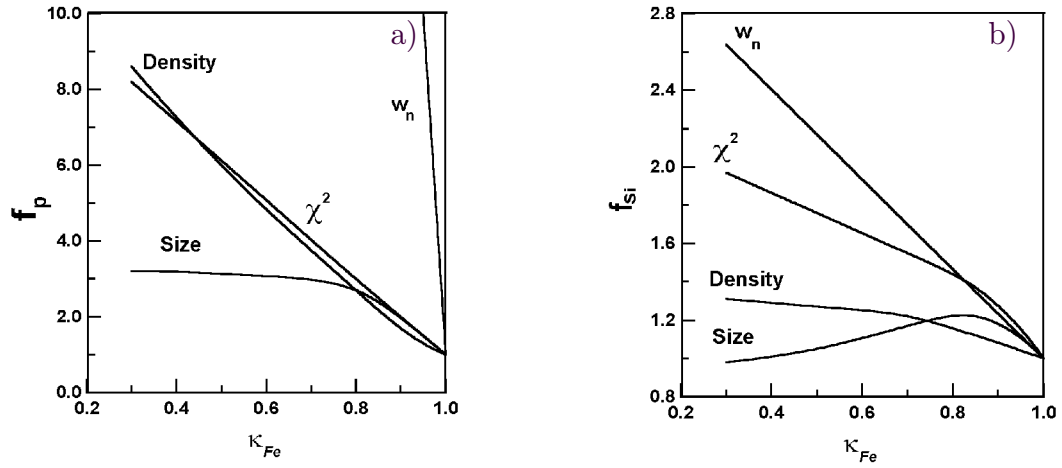

Figure 6. Results on an independent application of selection criteria for the IACT system. Iron nuclei against protons (a) and against silicon nuclei (b)

Table 5

The total effect of selection of the iron group of nuclei for a single IACT. Selection conditions: (400 ph. e. $< M < 1500$ ph. e.), ($D < 15$ ph. e.), ($0.4^o < l < 0.8^o$), ($0.3^o < w < 0.5^o$), ($2 * \chi^2 < \chi^2_o = 0.8$)

Number of group, j	1	2	3	4	5
Symbol of group	P	α	O	Si	Fe
κ_j^{Fe}	0.003	0.011	0.029	0.042	0.115
f_j^{Fe}	38.3	10.4	3.96	2.73	1.00
$\tilde{P}_j^{Fe}$	23.3	17.9	16.7	22.4	19.7
P_j	72.7	15.3	5.4	5.0	1.6

Table 6

The total effect of selection of the oxigen group of nuclei for a single IACT. Selection conditions: (350 ph. e. $< M < 1500$ ph. e.), ($D < 16$ ph. e.), ($0.4^o < l < 0.8^o$), ($0.25^o < w < 0.35^o$), ($2 * \chi^2 < \chi^2_o = 0.8$)

Number of group, j	1	2	3	4	5
Symbol of group	P	α	O	Si	Fe
κ_j^{Si}	0.006	0.020	0.055	0.057	0.068
f_j^{Si}	9.20	2.75	1.00	0.96	0.81
$\tilde{P}_j^{Si}$	30.5	21.3	20.7	19.9	7.6
P_j	72.7	15.3	5.4	5.0	1.6

ration of different components of the CRs. For a single telescope, the large uncertainty of the energy E_0 and of the core position R_0 of the shower results in an additional broadening of the distributions of the image parameters. Consequently this increases the overlaping domains from different nuclei. Therefore, one may expect that the separation efficiency of CR nuclei would be improved significantly if a method for determination of E_0 and R_0 on the *event-by-event* basis would be possible. In the imaging atmospheric Cherenkov technique this can be achieved by stereoscopic observations of showers by ≥ 2 IACTs. Furthermore, since the images of a shower in different projections only partially correlate with each other, the use of the image parameters from separated telescopes should significantly improve the efficiency of separation of different populations of the CR nuclei.

Geometrical reconstruction of the distance to the shower core by detection of the shower images by ≥ 2 separated telescopes with an accuracy of $\Delta R_0 \leq 30$ m allows an estimate of the primary energy E_0 based on the calculated Cherenkov light density profile. Such an estimate contains an obvious uncertainty connected with the atomic number of the primary particle which is *a priory* an unknown parameter. However, all selection criteria considered here are aimed at distinguishing a group of nuclei with a given value of the mean atomic number. Thus, including in the selection parameters the energy dependence corresponding exactly to the group assigned for selection (i.e. assuming a fixed atomic number A), one can expect an increase of the acceptance probability for this group and, consequently, an improvement of the separation efficiency.

In the case of stereoscopic observations of images,

when the parameters E_0 and R_0 are already determined, it is useful to apply a differential approach in the image analysis, namely to use, instead of the standard shape parameters, *Width (w)* and *Length (l)*, the so called *scaled* parameters:

$$w_n = w/\bar{w}^{(i)}(R_0, E_0)\,, \qquad (8)$$

where $\bar{w}^{(i)}(R_0, E_0)$ is the average calculated value (from Monte Carlo simulations) of the *Width* parameter for events of the nuclei group i assigned for selection.

To demonstrate this, we show in Figures 6 the efficiency of separation of the Fe group nuclei from the protons (Figure 6a) and from the nuclei of the Si group (Figure 6b), using an independent application of each selection criterion to the IACTs system. It is seen that in the case of suppression of protons the efficiency of the scaled w_n parameter is much higher than the efficiency of other parameters. In the case of neighbouring nuclei groups the other image parameters, in particular the χ^2-parameter, have a non-negligible impact on the separation procedure.

The results on the calculated efficiences, when selecting the iron and (CNO) groups, of CRs are presented in Tables 7 and 8. In Table 9 we compare the values of the enrichment factor for a single IACT and the IACTs system. From these results we may conclude that the separation efficiences of different group of nuclei are significantly larger in comparison with a single IACT. In particular, in the case of selection of iron nuclei, the protons and α-particles can be excluded practically completely. Furthermore, in the case of stereoscopic observations a considerable separation takes place even for the neighbouring groups, e.g. (CNO) nuclei against α-particles (see Table 9). It is important to note that the selected group in the case of stereoscopic observations becomes the most abundant component in the *residual* (after the imaging) detection rate. For example, in the case of selection of iron nuclei their percentage in the detection rate increases from 2.4% up to $\sim 70\%$.

6. Sensitivity of results to hadron interaction model

Any technique pretending to study the chemical composition of CRs by ground based detectors contains an uncertainty connected with the cross-sections of the interactions of heavy nuclei. Despite recent progress in this field, our knowledge about these interactions at very high energies is still based on a several model assumptions. Therefore it is important to analyse the sensitivity of the image

Table 7

The total effect of selection of the iron group of nuclei for the IACT system. Selection conditions: (M_1&$M_2 > 450$ ph. e.); (D_1&$D_2 < 20$ ph. e.), (w_{n1}&$w_{n2} > 0.90$), ($4 * \chi^2 < 1.4$)

Number of group, j	1	2	3	4	5
Symbol of group	P	α	O	Si	Fe
κ_j^{Fe}	0.000	0.000	0.010	0.013	0.152
f_j^{Fe}	∞	∞	15.2	11.7	1.00
$\tilde{P}_j^{Fe}$	0.0	0.0	13.7	16.6	69.7
P_j	67.1	16.8	7.2	6.7	2.4

Table 8

The total effect of selection of the oxygen group of nuclei for the IACT system. Selection conditions: (M_1&$M_2 > 400$ ph. e.), ($0.85 < w_{n1}$&$w_{n2} < 0.95$), ($4 * \chi^2 < 1.4$)

Number of group,j	1	2	3	4	5
Symbol of group	P	α	O	Si	Fe
κ_j^{CNO}	0.002	0.009	0.096	0.044	0.026
f_j^{CNO}	48.0	10.7	1.00	2.18	3.69
$\tilde{P}_j^{CNO}$	10.1	11.3	51.8	22.0	4.8
P_j	67.1	16.8	7.2	6.7	2.4

Table 9

Results on the enrichment factor η. Selection conditions are similar to Tables 6-8

	Single IACT		IACT system	
Selected nucleus group, i	Fe	O	Fe	O
κ_i	0.115	0.055	0.152	0.096
$\eta^{(i)}$	12.3	3.8	29.0	7.2

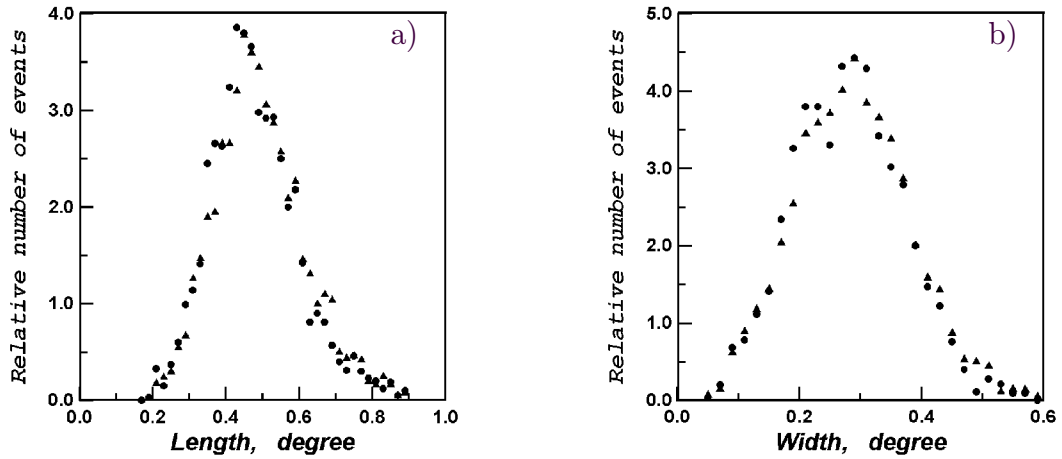

Figure 7. The probability distributions of *Lenght* (a) and *Width* (b) parameters for different models of hadron interactions. Primary oxigen nucleus, E =10 TeV. q_o =10 ph. e.. • – our simulation code

Table 10

The mean values and fluctuations of characteristics of γ-quanta generated in the air shower. Primary energy E=10 TeV. E_{th}=1 GeV. 1 — CORSIKA, 2 — our simulation code

Primary nucleus	P	P	O	O
Simulation code	1	2	1	2
$< E_{el}/E >$	0.558	0.497	0.343	0.380
$\delta(E_{el}/E)$	0.181	0.199	0.094	0.098
$< E_\gamma/N_\gamma >$,(GeV)	19.2	17.9	7.48	7.65
$< t_E >$, (g/cm^2)	239	212	145	181
$\delta(t_E)$	0.543	0.550	0.315	0.325
$< sin\theta_E >$	0.016	0.015	0.034	0.039
$\delta(sin\theta_E)$	0.362	0.327	0.125	0.122

parameters to the models for the hadron interactions. In the code [6,7], used in this paper, a modified version of the *radial scaling model* of hadron interactions [16] is implemented. For comparison we have simulated hadron cascades of air showers using the *dual parton model* version of the CORSIKA code [8]. For simulation of showers produced by heavy nuclei in both codes we have used the *fragmentation model* in which it is assumed that all overlapping nucleons of the projectile-nucleus interact with the target-nucleus independently from each other. For the non-overlapping part of the projectile a fragmentation takes place into nucleons, α-particles and heavier nuclei. To exclude differences in simulation results connected with the development of the electromagnetic cascades, and the production of the Cherenkov radiation, we have used only the hadronic part of the shower development of the CORSIKA code. In a first step the hadronic part of the air shower is simulated and the kinematic parameters of the produced photons, electrons and muons (the energy, momentum, time and point of production) are stored. In the second step all other simulations are carried out (the development of electromagnetic and muon components, the emission and transport of the Cherenkov light, the evaluation of image parameters, etc.). All simulations of the second step are carried out by means of the electromagnetic part of our simulation code.

In Table 10 we present values of the average (for one cascade) energy of emitted γ-rays, E_γ/N_γ, the portion of the primary energy, transferred to the electromagnetic component E_{el}/E, the depth of the *center of gravity* of energy transferred to γ-rays

$$t_E = \frac{\sum_{i=1}^{N_\gamma} t_{\gamma i} \cdot E_{\gamma i}}{\sum_{i=1}^{N_\gamma} E_{\gamma i}}, \qquad (9)$$

and the average *sine* of the emission angle of the energy transferred to γ-rays:

$$sin\theta_E = \frac{\sum_{i=1}^{N_\gamma} sin\theta_{\gamma i} \cdot E_{\gamma i}}{\sum_{i=1}^{N_\gamma} E_{\gamma i}}. \qquad (10)$$

In Table 10 we present also the fluctuations of these parameters. We emphasize the satisfactory agreement between both the mean values of parameters, and their fluctuations calculated by the two different codes. Thus, we expect good agreement also in the characteristics of the Cherenkov radiation. In Table 11 we present the results of calculations of the average values and fluctuations of the *Width* and *Length* parameters. In Figure 7 we show also the distributions of the *Width* and *Length*

Table 11

Data on the mean value and the mean squared deviation of the w- and l-parameters. E=10 TeV, q_o = 10 ph. e.. 1 — CORSIKA, 2 — our simulation code. All quantities are measured in degree

Primary nucleus	Code	$\bar{w}$	σ_w	$\bar{l}$	σ_l
P	1	0.219	0.093	0.525	0.133
P	2	0.214	0.090	0.550	0.127
O	1	0.276	0.095	0.481	0.124
O	2	0.287	0.097	0.498	0.131

parameters. Table 11, and Figure 7 demonstrate that both models of hadron interactions give very similar results for the parameters of the Cherenkov radiation.

Summary

The results discussed in this paper allow us to reach an optimistic conclusion concerning the potential of the imaging atmospheric Cherenkov technique for a study of the spectrum and chemical composition of CRs. For that purpose, the currently operating IACTs, like the Whipple 10 m telescope on Mt. Hopkins [1], or the HEGRA system of telescopes on La Palma [17], are already able to give interesting results in the energy region 1-100 TeV/amu. This energy region is below the energy threshold of air shower particle arrays. In addition, the statistics of the satellite- and balloon-borne experiments at these energies is rather limited.

The effective energy threshold of registration of air showers by an IACT increases rapidly with the atomic number of the primary nucleus. This circumstance reduces significantly the proportion of heavy nuclei in the IACT detection rate compared to their proportion in the primary cosmic radiation. Nevertheless even for the nuclei of the iron group the IACT technique yields an adequate statistics. In particular, for one year operation of IACT telescopes like the HEGRA IACT system we may expect more than 10^5 air showers produced by **VH** nuclei.

For the separation of air showers created by different primary nuclei by means of the IACT technique one needs image parameters sensitive to the atomic number of the nucleus. Our study shows that a number of image parameters exhibit this sensitivity. The most distinctive of them are the *Width* of the image and the intrinsic fluctuations of the image light intensity.

While the proton component of the cosmic radiation can be well separated on the basis of the *Width* parameter already for a single imaging telescope, the separation of other nuclei becomes effective only for IACT systems. Particularly in the case of selection of **VH** nuclei a simple IACT system consisting of two identical telescopes gives the possibility to increase the percentage of these nuclei in the total detection rate from $\sim 2\%$ to $\sim 70\%$. For comparison, a single IACT gives only a comparable percentage of the VH and other groups of nuclei. It is expected that the separation efficiency of nuclei of different groups will be noticeably improved with adding more telescopes to the system.

Appendix: The χ^2 parameter in the image analysis

In the process of IACT observations, air showers are registered that have a wide range of primary energies and core locations. The primary energy, E, and the core location, R_o, influence the magnitude, size and shape of the image. As a consequence some additional fluctuations, not connected with the nature of the primary particle, are introduced in the distribution of the image light intensity. For a successful application of intrinsic fluctuations to the separation of air showers one should diminish these 'unwanted' fluctuations. In principle, this can be acchieved by taking into account the dependence of selection criteria on E and R_o, but a single IACT does not provide us with these quantities. For this purpose we use in our analysis an alternative approach aimed to reduce the dependence of the selection criteria on the image parameters (*Size, Width* and *Length*) correlating essentially with the quantities E and R_o. It is described as follows:

Let us locate the origin O of the XYZ coordinate system in the centre of gravity of the image and denote as $\rho(x, y)$ the density of the image light intensity in the focal plane of the IACT optical reflector. Let us also consider the l- and w-parameters as a measure of distance along the major (X) and the minor (Y) image axes. As a result we come to a modified distribution function

$$\phi(u, v) = (l \cdot w \cdot Size)^{-1} \cdot \varrho(x, y)$$
$$\int du \int dv \ \phi(u, v) = 1, \qquad \text{(A1)}$$
$$u = x/l, v = y/w,$$

whose values for fixed u, v correlate with $Size, Length$ and $Width$ (and, consequently, with E and R_o) essentially weaker than does the initial density $\rho(x, y)$.

Table A 1

Fluctuations of quantities N_l, N_w. The selection criteria are the following: (200 ph. e.< M <1000 ph. e.), ($0.3° < l < 0.7°$), ($0.2° < w < 0.4°$); $\Delta_u = \Delta_v = 0.15$, K = 10

k		1	3	5	7	9
$u_k(v_k)$		-0.75	-0.45	-0.15	0.15	0.45
$\delta N_{l,k}$	P	0.38	0.28	0.24	0.20	0.22
	O	0.30	0.21	0.18	0.16	0.17
	Fe	0.27	0.16	0.12	0.11	0.13
$\delta N_{w,k}$	P	0.26	0.22	0.21	0.23	0.27
	O	0.20	0.16	0.15	0.15	0.18
	Fe	0.14	0.12	0.11	0.11	0.13

The two-dimensional density $\phi(u,v)$ could be characterized by two one-dimensional functions $\phi_l(u)$ and $\phi_w(v)$ which are the projections of $\phi(u,v)$ to the corresponding coordinate axes.

$$\phi_l(u) = \int \phi(u,v)dv, \qquad \phi_w(v) = \int \phi(u,v)du \tag{A2}$$

In turn the functions $\phi_l(u)$ and $\phi_w(v)$ can be parametrized by a number of integrals over Δu and Δv bins:

$$N_{l,k} = \int_{u_k}^{u_{k+1}} \phi_l(u)u_{k+1} = u_k + \Delta u, \quad k = 1,2,\cdots,K, \tag{A3}$$

$$N_{w,k} = \int_{v_k}^{v_{k+1}} \phi_w(v)dv, v_{k+1} = v_k + \Delta v, \quad k = 1,2,\cdots,K \tag{A4}$$

The set of integrals N_w and N_l determine the image profile in the longitudinal and transverse directions. Thus, fluctuations in the image shape reflect themselves in the fluctuations of the integrals N_w and N_l.

In Table A1 we show the data on the fluctuations of quantities N_l, N_w calculated assuming the primary energy spectrum (1). One can see that the *normalized* fluctuations in the image shape correlate significantly with the atomic number of the primary nucleus. In particular, the difference in fluctuations corresponding to protons and iron nuclei is as large as a factor of ~ 2. To construct the selection criteria dealing with the image fluctuations we calculate a set of mean values and mean squared deviations of the quantities $N_{l,k}$, $N_{w,k}$, $k = 1,2,\cdots,K$ (see (A3,A4)) corresponding to the group of nuclei assigned for selection. After that, for detected images from overall data sample, we calculate the χ^2 value according to the following expression:

$$\chi^2_t = K^{-1} \cdot \sum_{k=1}^{K} \{(N_{t,k} - \bar{N}^{(i)}_{t,k})/\sigma_{N^{(i)}_{t,k}}\}^2, \quad t = l,w. \tag{A5}$$

The separation of the chosen nuclei (i) from the other nuclei could be performed using the simple *cut* on the χ^2 parameter:

$$\chi^2_t < \chi^2_o, \quad t = l,w. \tag{A6}$$

Note that for a number of telescopes we apply simultaneously this cut for all detected images.

To understand the meaning of the selection parameter (A5) let us calculate the mean value of χ^2 for an arbitrary nuclei group (j):

$$\bar{\chi^2_t} = K^{-1} \cdot \sum_{k=1}^{K} \{[\sigma N^{(j)}_{t,k}/\sigma N^{(i)}_{t,k}]^2 + [(\bar{N}^{(j)}_{t,k} - \bar{N}^{(i)}_{t,k})/\sigma N^{(i)}_{t,k}]^2\}, \quad t = l,w. \tag{A7}$$

Because of the renormalization of the distribution (A2) the integrals $\bar{N}_t$ depend only weakly on the atomic number (i.e. $\bar{N}^{(i)} \simeq \bar{N}^{(j)}$) and that is why the first term in the right-hand side of equation (A7) gives the main contribution to the $\bar{\chi^2_t}$ parameter. At the same time $\sigma N^{(j)}$ decreases with j (see Table A1, the index j runs up while the nuclei atomic number increases). Consequently, $\bar{\chi^2_t}$ also decreases with j, and the probability distribution of χ^2_t becomes more narrow. Thus to select the images corresponding to small values of χ^2_t one can reject air showers which belong to nuclei groups with numbers $j < i$, where the index i corresponds to the assigned nuclei group.

Note that in general the χ^2 parameter depends on values of parameters Δu, Δv, K. However the present analysis shows that the efficiency of nuclei separation is quite insensitive to the exact values of these parameters. Everywhere in analysis (except for Table A1) we use the following values $\Delta u = \Delta v = 0.15$, $K = 40$.

References

1. Cawley M. and Weekes T. // Exp. Astr., 1995, v.6, p.7.
2. Hillas A. M. // Space Science Reviews, 1996, v.75, Nos.1-2., p.17.
3. Swordy S. // Proc. 23-rd ICRC, Calgary, 1993, v.2, p.125.
4. Lindner A. et.al. // Proc. 24-th ICRC, Rome, 1995, v.1, p.422.
5. Fegan D. J. // Space Science Reviews, 1995, v.75, Nos.1-2., p.137.
6. Plyasheshnikov A. et.al. Preprint Lebedev Phys. Inst., Moscow, 1989, 92, 48 p.
7. Konopelko A. et.al. Preprint Lebedev Phys. Inst. (in Russian), Moscow, 1992, v.6, 48 p.
8. Capdevielle J. et.al. Preprint KfK, Karlsruhe, 1992, 4998, 54 p.
9. Aharonian F. et.al. // J. Phys. G: Nucl. Part. Phys. v.21. pp.985-993.
10. Hillas A. M. // Proc. 19-th ICRC, La Jolla, 1985, v.1, p.155.
11. Wiebel B. Preprint WUB-94-08, Wuppertal, 1994, 47 p.
12. Aharonian F. et.al. // J. Phys. G: Nucl. Part. Phys., 1995, 1995, v.21, p.419.
13. Schatz G. et.al. // J. Phys. G: Nucl. Part. Phys., 1994, v.20, p.1267.
14. Zatsepin V. et.al. // Proc. 23-rd ICRC, Calgary, 1993, v.2, p.1.
15. Asakimori K. et.al. // Proc. 23-rd ICRC, Calgary, 1993, v.2, p.25.
16. Hillas A. M. // Proc 16-th ICRC, Kyoto, 1979, v.6, p.13.
17. Aharonian F. et.al. // Proc. International Workshop "Towards a Major Atmospheric Cherenkov Detector II", Calgary, 1993, ed. by R. C. Lamb p.81.